axioms

MDPI

Article

A Novel Method for Designing Multistable Systems with a Hidden Attractor

Rodolfo de Jesús Escalante-González [1,*], Hector Eduardo Gilardi-Velázquez [2] and Eric Campos [3]

[1] Departamento de Eléctrica, Electrónica, Mecatrónica y Semiconductores, Tecnológico Nacional de México, Campus San Luis Potosí, Avenida Tecnológico, Soledad de Graciano Sánchez 78437, San Luis Potosí, Mexico
[2] Facultad de Ingeniería, Universidad Panamericana, Josemaría Escrivá de Balaguer 101, Aguascalientes 20296, Aguascalientes, Mexico; hgilardi@up.edu.mx
[3] División de Control y Sistemas Dinámicos, Instituto Potosino de Investigación Científica y Tecnológica, A.C., Camino a La Presa San José 2055, Lomas 4 Sección, San Luis Potosí 78216, San Luis Potosí, Mexico; eric.campos@ipicyt.edu.mx
* Correspondence: rodolfo.eg@slp.tecnm.mx

Abstract

Dynamical systems with chaotic attractors are an interesting topic not only for their complex behavior but also due to their potential applications. Along with the chaos, systems can also present interesting features such as multistability, global basin of attractions, entangled basins of attraction, etc. The existence of chaotic systems with multistable hidden attractors increases complexity but also the number of potential applications. Several systems with hidden attractors have already been found by numerical search; however, it is usually not possible to substantially modify their equations or attractor geometry. In this study, an approach to generate multistable systems with a class of hidden attractors is proposed. The approach allows for the control of the amplitude and frequency of the chaotic signals of the different attractors as well as their location in the space by preserving a simple matrix form in the vector field. Particular cases with mono-stability and multistability are shown. Also, chaotic signals obtained through the approach are used in a pseudorandom number generator to obtain binary sequences which are tested under the Statistical Test Suite for Random and Pseudorandom Number Generators for Cryptographic Applications provided by the National Institute of Standards and Technology (NIST).

Keywords: hidden attractor; multiscrolls; multistability; chaotic system; dynamical analysis

MSC: 65P20

Academic Editor: José Manoel Balthazar

Received: 29 January 2026
Revised: 12 February 2026
Accepted: 17 February 2026
Published: 27 February 2026

1. Introduction

Since Edward Lorenz's early work in the 1960s, the study of chaotic dynamical systems has profoundly transformed the understanding of nonlinear phenomena in nature [1]. Numerous chaotic and nonlinear dynamical systems were identified in disciplines as diverse as physics [2,3], biology [4], engineering, and economics, consolidating the concept of strange attractors as geometric structures that govern the dynamics of these systems [5]. Research focused primarily on self-excited attractors, those that can be easily located from initial trajectories near unstable equilibrium points [6]. However, recent theoretical advances have revealed the existence of a new class of dynamic behaviors, namely hidden attractors [7]. Chaotic attractors generated in vector fields without equilibria fulfill the hidden attractor definition [8].

A dynamical system (T, X, ϕ) where T is the evolution time, X is the phase space, and $\phi(\mathbf{x}, t)$ is the evolution function associated to a vector field $\dot{\mathbf{x}} = f(\mathbf{x})$ can present attractors of different types. According to [9], we can find two classes of attractors; one type is given by those well-known attractors excited from unstable equilibria (an equilibrium point satisfies $\{\mathbf{x} \in \mathbb{R}^n \mid 0 = f(\mathbf{x})\}$) called *self-excited attractors*. In this kind of attractor, the basin of attraction intersects with an arbitrarily small open neighborhood of equilibria [10] and from a numerical point of view, they are easy to find by testing initial conditions close to the unstable equilibria. The second class is known as *hidden attractors*, whose basin of attraction does not contain neighborhoods of equilibria. This class is harder to find since testing initial conditions near the equilibrium (if any) does not necessarily generate trajectories that converge to a hidden attractor. An attractor is called a self-excited attractor if its basin of attraction intersects with any open neighborhood of an unstable fixed point. Otherwise, it is called a hidden attractor [10].

Although numerous examples of hidden attractors have been reported in various types of dynamical systems in recent years [11–13], a deep understanding of the mechanisms that lead to their generation remains an open challenge [7,14]. In contrast to self-excited attractors, whose appearance can be associated with local bifurcations and trajectories emanating from unstable equilibrium points [6], hidden attractors emerge from global system interactions that are not directly linked to these equilibria [5]. This characteristic makes not only their detection difficult but also the systematic design of models capable of exhibiting this type of behavior. Consequently, the study of the structural and topological conditions that favor the emergence of hidden attractors is currently one of the most active and challenging lines of research within modern chaos theory and nonlinear systems [7]. According to these definitions, a hidden attractor could be observed in systems without equilibria or even systems with only a stable equilibrium point. They could also be found in more complex systems with different kinds of equilibria and even in coexistence with other hidden and self-excited attractors in what are known as multistable systems. In dynamical systems, the phenomenon of multistability refers to the coexistence of multiple final stable states, whether they are equilibrium points, periodic orbits, or hidden attractors, where the convergence to each of the possible final states depends only on the initial condition of the system [5].

After the reported double-scroll attractor in Chua's circuit, there has been a constant interest in the generation of double-scroll and multiscroll attractors. Some approaches for the generation of self-excited scroll attractors are found in [15–17]. The phenomenon of multistability has attracted considerable interest in a variety of fields. This phenomenon has been found in integer-order multiscroll systems and has been studied in several papers using different mechanisms, i.e., by eigenspectra variation in a piecewise linear (PWL) system [18,19], by applying control techniques that produce the coexistence of multiple attractors [20] or by changing the location of the equilibrium point by a bifurcation parameter that induces bistable behavior [21,22]. In fractional-order systems, the phenomenon of multistability has also been described [23,24], with these studies ranging from systems with no equilibrium points to systems based on memristors and systems that can have a family of bistable attractors [25].

Some recent studies have explored the use of chaotic attractors in cryptographic applications; for instance, in [26], a memristor-based multiscroll Hopfield neural network with a non-polynomial memristor is proposed and implemented using a field-programmable gate array (FPGA); an encryption circuit is also proposed. In [27], a novel five-dimensional Hopfield neural network system is introduced by replacing the self-synapse of a single neuron with a cosine memristor model. The system was implemented using FPGA, has ifinitely many equilibria, and generates an arbitrary number of multi-scroll attractors. Due to its rich

dynamics, it was used to produce random sequences for image encryption. In [28], a new hyperchaotic map is proposed as well as a multi-image encryption algorithm that employs a hierarchical significance-aware encryption strategy. In [29], the authors introduce a novel 2D hyperchaotic fractional-order map and develop a cryptographic scheme algorithm. In [30], a chaotic image encryption scheme is presented, which is based on vector-level operations and a two-dimensional enhanced logistic modular map. Strange attractors in which the trajectories exhibit a wrapping or unwrapping that resembles the solutions near a focus equilibrium point are usually called scroll attractors. Chaotic scroll attractors have been studied for some decades and have been largely used in the design of pseudorandom number generators, such as the one reported in [31,32]. The ability to reconstruct attractors in certain chaotic systems presents a security risk for encryption algorithms, as it enables potential system recovery [33]. The reconstruction of the hidden scroll attractor is harder.

The main contributions of this paper are as follows:

- An approach for the generation of a self-excited double-scroll chaotic attractor is introduced. The vector field presents a matrix with the form found in classical systems in a controllable canonical form, which is usually preferred over other forms due to its simplicity in electronics implementations. In contrast to other reported systems with scroll attractors and this type of matrix, the reported approach has a wider range of eigenspectra that produce attractors. Also, chaos in the sense of Shilnikov is guaranteed.
- An approach for the generation of a bistable system with only self-excited attractors and multistable systems with two self-excited double-scroll attractors and one hidden double-scroll attractor is then presented. The method allows for the control of the amplitude and frequency of the chaotic signals of the different attractors as well as their location in the space by preserving a simple matrix form in the vector field.
- The approach is further extended to multistable systems with a coexistence of self-excited attractors and a hidden attractor in 1D, 2D, and 3D grid attractors.

The rest of this study is organized as follows: in Section 2, the new approach for the generation of a self-excited double-scroll chaotic attractor is introduced. In Section 3, an approach for the generation of bistable and multistable systems with three attractors is presented. In Sections 4 and 5, the method is extended to the generation of 1D, 2D, and 3D grid hidden attractors. In Section 6, a known binary sequence generator algorithm is used along with a particular case of a multistable system generated with the approach to be tested in the test suite provided by the National Institute of Standards and Technology (NIST). Finally, in Section 7, there is a concluding discussion.

2. System Design Approach

Let $X \subset \mathbb{R}^3$ and $P = \{P_1, P_2\}$ $(\eta > 1)$, with $X = P_1 \cup P_2$ and $P_1 \cap P_2 = \emptyset$, be a space and a partition, respectively. Let us also consider that there exists a saddle equilibrium point in each atom P_i. Let us consider a PWL system $T : X \to X$, whose vector field is given by

$$\dot{\mathbf{x}} = A\mathbf{x} + f(\mathbf{x})B, \tag{1}$$

where $\mathbf{x} = (x_1, x_2, x_3)^T \in \mathbb{R}^3$ is the state vector and A is a linear operator given by

$$A = \begin{bmatrix} 0 & 1 & 0 \\ 0 & 0 & 1 \\ (b^2 + a^2)c & -2ac - b^2 - a^2 & c + 2a \end{bmatrix}, \tag{2}$$

with $a, b, c \in \mathbb{R}$ such that $a, b > 0$ and $c < 0$ and whose complexification $A^{\mathbb{C}}$ has the eigenvalues $\lambda_1 = c$, $\lambda_2 = a + ib$ and $\lambda_3 = a - ib$. B is a constant vector given by

$$B = \frac{1}{3}\begin{bmatrix} a - 2c \\ a^2 - 2c^2 - b^2 \\ a^3 - 2c^3 - 3ab^2 \end{bmatrix}, \tag{3}$$

f is a function defined as

$$f(\mathbf{x}) = \begin{cases} -\alpha, \text{ if } & \mathbf{x} \in P_1; \\ \alpha, \text{ if } & \mathbf{x} \in P_2; \end{cases} \tag{4}$$

where $\alpha \in \mathbb{R}$ and $\alpha > 0$. The equilibria are given by $\mathbf{x}^*_{eq_i} = (x^*_{1_{eq_i}}, x^*_{2_{eq_i}}, x^*_{3_{eq_i}})^T = -f(\mathbf{x})A^{-1}B \in P_i$, with $i = 1, 2$. Let us consider the switching surface defined as follows:

$$SW = \{\mathbf{x} \in \mathbb{R}^3 : \mathbf{x}^T n_\alpha = 0\}, \tag{5}$$

$$P_1 = \{\mathbf{x} \in \mathbb{R}^3 \,|\mathbf{x}^T n_\alpha < 0\} \cup \{\mathbf{x} \in SW : \mathbf{x}^T n_3 \geq 0\}, \tag{6}$$

$$P_2 = \{\mathbf{x} \in \mathbb{R}^3 \,|\mathbf{x}^T n_\alpha > 0\} \cup \{\mathbf{x} \in SW : \mathbf{x}^T n_3 < 0\}, \tag{7}$$

where

$$\mathbf{n}_3 = \frac{1}{3}\begin{bmatrix} 4 \\ 2c + 2a \\ 2c^2 - 2b^2 + 2a^2 \end{bmatrix}, \tag{8}$$

$$\mathbf{n}_\alpha = \begin{bmatrix} -2bc^2 + 4abc + b^3 + a^2 b \\ -6ab \\ 3b \end{bmatrix}. \tag{9}$$

The parameter α controls the amplitude of the oscillation in the self-excited attractors, the parameter b controls the frequency, and a controls the time spent by a trajectory in each atom of the partition P.

For the appropriate selection of parameters a, b, c, and α such that the Shilnikov inequality $|c| > |a| > 0$ is fulfilled, the system exhibits a self-excited attractor. The saddle index for the equilibria is $\nu = |\frac{a}{c}| < 1$. Moreover, the self-excited attractor presents Shilnikov chaos, which can be analytically proven.

If it were desired to implement the system with analog devices, the switching rule given by (5) could be implemented by using an operational amplifier using the technique reported in [34] followed by a comparator whose inverting terminal is connected to zero.

Proposition 1. *Given a system of the form* (1), (2), (3), *and* (4), *there exists a heteroclinic cycle whose intersection points with the switching surfaces are given by*

$$\mathbf{x}_{in_1} = -\alpha\begin{bmatrix} 1 & \frac{2c+a}{3} & \frac{2c^2-b^2+a^2}{3} \end{bmatrix}^T, \tag{10}$$

$$\mathbf{x}_{in_2} = \alpha\begin{bmatrix} 1 & \frac{2c+a}{3} & \frac{2c^2-b^2+a^2}{3} \end{bmatrix}^T, \tag{11}$$

Proof. There exists a matrix Q

$$Q = \begin{bmatrix} 1 & 0 & 1 \\ c & b & a \\ c^2 & 2ab & a^2 - b^2 \end{bmatrix}, \tag{12}$$

such that

$$J = Q^{-1}AQ, \tag{13}$$

where J is a matrix of the form

$$J = \begin{bmatrix} c & 0 & 0 \\ 0 & a & -b \\ 0 & b & a \end{bmatrix}. \tag{14}$$

The equilibrium points $\mathbf{x}_1^*$ and $\mathbf{x}_2^*$ are symmetric with respect to the origin. Let us consider the transformation

$$\mathbf{z}^{(\mathbf{i})} = Q^{-1}(\mathbf{x} - \mathbf{x}_i^*) \text{ for } i \in \{1, 2\}, \tag{15}$$

Changing the coordinates of $\mathbf{x}_{in_2}$ to $\mathbf{z}^{(\mathbf{2})}$, we get

$$Q^{-1}(\mathbf{x}_{in_2} - \mathbf{x}_1^*) = \begin{bmatrix} \frac{4\alpha}{3} & 0 & 0 \end{bmatrix}^T, \tag{16}$$

which along with the shape of (14) implies it belongs to the stable manifold of the system $\dot{\mathbf{z}}^2 = J\mathbf{z}^2$. The matrix in (14) is in Jordan blocks, so it can be seen that the vectors of the form $[\rho, 0, 0]^T$ with $\rho \in \mathbb{R}$ belong to the eigenspace whose associated eigenvalue is $\lambda = c < 0$. Therefore, they belong to the stable manifold and then

$$\lim_{t\to\infty} \varphi(\mathbf{x}_{in_2}, t) = \mathbf{x}_1^*. \tag{17}$$

In the same way

$$Q^{-1}(\mathbf{x}_{in_1} - \mathbf{x}_2^*) = \begin{bmatrix} -\frac{4\alpha}{3} & 0 & 0 \end{bmatrix}^T, \tag{18}$$

$$\lim_{t\to\infty} \varphi(\mathbf{x}_{in_1}, t) = \mathbf{x}_2^*. \tag{19}$$

Now, let us change the coordinates of $\mathbf{x}_{in_1}$ to $\mathbf{z}^{(\mathbf{1})}$. We get

$$Q^{-1}(\mathbf{x}_{in_1} - \mathbf{x}_1^*) = \begin{bmatrix} 0 & 0 & -\frac{2\alpha}{3} \end{bmatrix}^T, \tag{20}$$

which along with the shape of (14) implies that it belongs to the unstable manifold of the system $\dot{\mathbf{z}}^1 = J\mathbf{z}^1$ in the same way as

$$Q^{-1}(\mathbf{x}_{in_2} - \mathbf{x}_2^*) = \begin{bmatrix} 0 & 0 & \frac{2\alpha}{3} \end{bmatrix}^T, \tag{21}$$

and thus it also belongs to the unstable manifold of the system $\dot{\mathbf{z}}^2 = J\mathbf{z}^2$. Now, from (6) and (16), the switching surface SW_1 is the set

$$SW_1 = \{\mathbf{x} \in \mathbb{R}^3 \mid \mathbf{x}^T\mathbf{n}_\alpha = 0\}, \tag{22}$$

Changing SW_1 to $\mathbf{z}^1$ gives

$$Q^{-1}(SW_1 - \mathbf{x}_1^*) = \left\{\mathbf{z}^{(1)} \mid z_1^{(1)} - 2z_3^{(1)} = \frac{4\alpha}{3}\right\}, \tag{23}$$

and changing SW_1 to $\mathbf{z}^2$ gives

$$Q^{-1}(SW_1 - \mathbf{x}_1^*) = \left\{\mathbf{z}^{(2)} \mid z_1^{(2)} - 2z_3^{(2)} = -\frac{4\alpha}{3}\right\}. \tag{24}$$

From the SW_1 transformed to $\mathbf{z}^{(1)}$ and $\mathbf{z}^{(2)}$, it can be concluded that the unstable manifold intersects SW_1 in a parallel direction from $z_2^{(1)}$ and $z_2^{(2)}$. Then, analyzing the uncoupled system in $z_2^{(i)}$ coordinates with $i \in \{1,2\}$, we have

$$\dot{z}_2^{(i)} = az_2^{(i)} - bz_3^{(i)}, \tag{25}$$

$$\dot{z}_3^{(i)} = bz_2^{(i)} - az_3^{(i)}, \tag{26}$$

$$\left(\dot{z}_2^{(i)}\right)^2 + \left(\dot{z}_3^{(i)}\right)^2 = a\left(\left(z_2^{(i)}\right)^2 + \left(z_3^{(i)}\right)^2\right), \tag{27}$$

If $r^2 = (z_2^{(i)})^2 + (\dot{z}_3^{(i)})^2$, then $r\dot{r} = ar^2$

$$\dot{r} = ar, \tag{28}$$

$$r = r_0 e^{(at)}. \tag{29}$$

but since $a < 0$ and the location of SW_1, it can be concluded that

$$\lim_{t\to-\infty} \varphi(\mathbf{x}_{in_1}, t) = \mathbf{x}_1^*, \tag{30}$$

$$\lim_{t\to-\infty} \varphi(\mathbf{x}_{in_2}, t) = \mathbf{x}_2^*, \tag{31}$$

which completes the heteroclinic cycle of P_1 and P_2. □

An illustration of one of the heteroclinic cycles is shown in Figure 1.

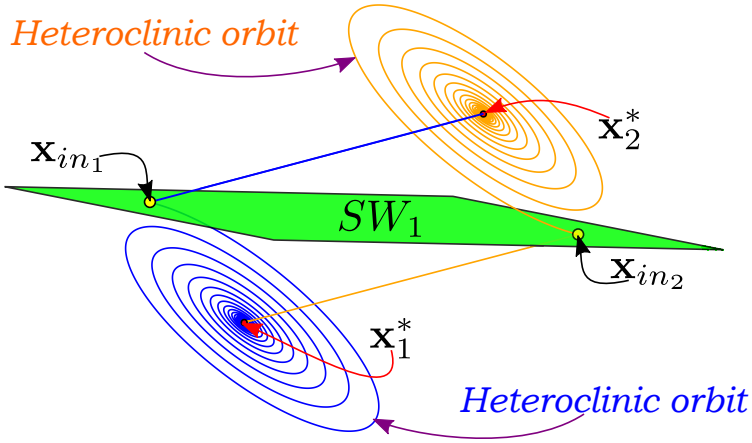

Figure 1. Illustration of the geometry of the system to guarantee the existence of a heteroclinic cycle. In blue and orange are the two heteroclinic orbits; in green is the switching surface.

In order to plot the heteroclinic loop in P_1 and P_2, we can find a point of each heteroclinic orbit close to the equilibrium point $\mathbf{x}_1^*$ as follows:

$$\mathbf{x}(0)_1 = \frac{1}{3}\begin{bmatrix} -2\alpha \\ -2a\alpha \\ (2b^2 - 2a^2)\alpha \end{bmatrix} e^{-\frac{2na\pi}{b}} + \mathbf{x}_1^*, \tag{32}$$

$$\mathbf{x}(0)_1 = -\frac{1}{3}\begin{bmatrix} -2\alpha \\ -2a\alpha \\ (2b^2 - 2a^2)\alpha \end{bmatrix} e^{-\frac{2na\pi}{b}} + \mathbf{x}_2^*, \tag{33}$$

where $n \in \mathbb{N}$ determines the number of turns a trajectory with an initial condition close to an equilibrium point performs before it reaches a switching surface. Therefore, the higher n is, the closer the initial condition is to the equilibrium point.

Let us consider a system of the form (1), (3), and (4) along with the parameter values $a = 0.2, b = 5, c = -3$, and $\alpha = 1$. The system presents a heteroclinic cycle and a double-scroll chaotic attractor shown in Figure 2.

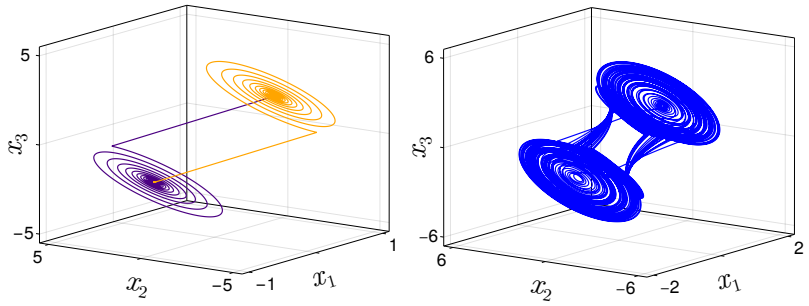

(**a**) (**b**)

Figure 2. (**a**) In orange and purple is the heteroclinic cycle of the system (1), (3), (4), and (5) for the parameters $a = 0.2$, $b = 5$, $c = -3$, and $\alpha = 1$. (**b**) In blue is the double-scroll self-excited chaotic attractor.

It is worth mentioning that flexible control over the amplitude and frequency of chaotic signals from self-excited attractors is achieved by expanding the set of parameter values that generate attractors. In traditional approaches based simply on fixed switching surfaces and saturation-type functionals, the set of selectable values is smaller, thus limiting this control.

3. Multistable System

Let

$$\dot{\mathbf{x}} = f(\mathbf{x}) = A\mathbf{x} + g(\mathbf{x}),\ \mathbf{x}(0) = \mathbf{x}_0, \tag{34}$$

be the associated vector field of an autonomous dynamical system, where $\mathbf{x} \in \mathbb{R}^n$, $A = \{a_i j\}_{i,j=1}^n \in \mathbb{R}^{n\times n}$, $a_{i,j} \in \mathbb{R}$, and $g : \mathbb{R}^n \to \mathbb{R}^n$. According to [19], the generalized multistability can be defined as follows:

Definition 1. *We say that the dynamical system given by* (34) *is generalized multistable if there exists more than one basin of attraction.*

In order to modify the previous approach for a multistable system with two double-scroll self-exited attractors and one hidden attractor, let $X \subset \mathbb{R}^3$ and $P = \{P_1, \ldots, P_\eta\}$ $(\eta = 4)$ with $X = \bigcup_{1\le i\le\eta} P_i$, and $P_i \cap P_j = \emptyset$ for $i \neq j$ be the phase space and a partition, respectively. Let us also consider that there exists a saddle equilibrium point in each atom P_i. Let us define two step functionals g and u as follows:

$$u(\tau) = \begin{cases} 1, & \text{if } \tau \ge 0; \\ -1, & \text{if } \tau < 0; \end{cases} \tag{35}$$

$$g(\tau,\zeta) = \begin{cases} 1, & \text{if } \tau > 0 \text{ and } \zeta \ge 0; \\ -1, & \text{if } \tau \le 0 \text{ and } \zeta \ge 0; \\ 1, & \text{if } \tau \ge 0 \text{ and } \zeta < 0; \\ -1, & \text{if } \tau < 0 \text{ and } \zeta < 0. \end{cases} \tag{36}$$

Please note that the difference between $u(\tau)$ and $g(\tau,\zeta)$ is just that the second one considers two variables; however, both functionals return only 1 or -1.

Consider the new $f(X)$ defined as

$$f(\mathbf{x}) = \alpha g((\mathbf{x} - f_1\mathbf{n}_1)^T\mathbf{n}_\alpha, \mathbf{x}^T\mathbf{n}_3) + f_1, \tag{37}$$

$$f_1 = \gamma u(\mathbf{x}^T\mathbf{n}_\gamma), \tag{38}$$

$$\mathbf{n}_\gamma = \begin{bmatrix} -2bc^2 + 4abc + 2b^3 + 2a^2b \\ -8ab \\ 4b \end{bmatrix}, \tag{39}$$

$$\mathbf{n}_1 = \frac{1}{3}\begin{bmatrix} 1 \\ 2c - a \\ 2c^2 + b^2 - a^2 \end{bmatrix}, \tag{40}$$

with $\gamma > 0$. The definition of parameters and equations arises from the design of the system for the location and geometric modification of the eigenspaces of matrix A. Although the analysis for its construction was carried out numerically, a structure with a wide range of attractors is presented. In the case of the equations u and g, these are step functionals responsible for partitioning the space and thus generating the switching surfaces. The vector $\mathbf{n}_\gamma$ is the normal vector to the switching surface at the origin. The vector $\mathbf{n}_1$ lies on the line along which the scroll attractors can be separated. The partition P has four atoms and three switching surfaces:

$$\begin{aligned} SW_1 &= cl(P_1) \cap cl(P_2), \\ SW_2 &= cl(P_2) \cap cl(P_3), \\ SW_3 &= cl(P_3) \cap cl(P_4), \end{aligned} \tag{41}$$

$$\begin{aligned} SW_1 &= \{\mathbf{x} \in \mathbb{R}^3 : (\mathbf{x} + \gamma\mathbf{n}_1)^T\mathbf{n}_\alpha = 0\}, \\ SW_2 &= \{\mathbf{x} \in \mathbb{R}^3 : \mathbf{x}^T\mathbf{n}_\gamma = 0\}, \\ SW_3 &= \{\mathbf{x} \in \mathbb{R}^3 : (\mathbf{x} - \gamma\mathbf{n}_1)^T\mathbf{n}_\alpha = 0\}, \\ &\{\mathbf{x} \in \mathbb{R}^3 : \mathbf{x}^T\mathbf{n}_3 \geq 0\} \cap SW_i \in P_i, \\ &\{\mathbf{x} \in \mathbb{R}^3 : \mathbf{x}^T\mathbf{n}_3 < 0\} \cap SW_1 \in P_{i+1}, \end{aligned} \tag{42}$$

$$P_1 = \{\mathbf{x} \in \mathbb{R}^3 \,|(\mathbf{x} - \gamma\mathbf{n}_1)^T\mathbf{n}_\alpha < 0\} \cup \{\mathbf{x} \in SW_1 : \mathbf{x}^T\mathbf{n}_3 \geq 0\}, \tag{43}$$

$$\begin{aligned} P_2 = \{\mathbf{x} \in \mathbb{R}^3 \,|(\mathbf{x} - \gamma\mathbf{n}_1)^T\mathbf{n}_\alpha > 0 \wedge \mathbf{x}^T\mathbf{n}_\gamma < 0\}, \\ \cup\{\mathbf{x} \in SW_1 : \mathbf{x}^T\mathbf{n}_3 < 0\} \cup \{\mathbf{x} \in SW_2 : \mathbf{x}^T\mathbf{n}_3 \geq 0\}, \end{aligned} \tag{44}$$

$$\begin{aligned} P_3 = \{\mathbf{x} \in \mathbb{R}^3 \,|(\mathbf{x})^T\mathbf{n}_\gamma > 0 \wedge (\mathbf{x} + \gamma\mathbf{n}_1)^T\mathbf{n}_\alpha < 0\}, \\ \cup\{\mathbf{x} \in SW_2 : \mathbf{x}^T\mathbf{n}_3 < 0\} \cup \{\mathbf{x} \in SW_3 : \mathbf{x}^T\mathbf{n}_3 \geq 0\}, \end{aligned} \tag{45}$$

$$P_4 = \{\mathbf{x} \in \mathbb{R}^3 \,|(\mathbf{x} + \gamma\mathbf{n}_1)^T\mathbf{n}_\alpha > 0\} \cup \{\mathbf{x} \in SW_3 : \mathbf{x}^T\mathbf{n}_3 < 0\}, \tag{46}$$

The equilibria is then located at

$$\mathbf{x}_1^* = (-\alpha - \gamma)\mathbf{n}_1, \tag{47}$$

$$\mathbf{x}_2^* = (\alpha - \gamma)\mathbf{n}_1, \tag{48}$$

$$\mathbf{x}_3^* = (-\alpha + \gamma)\mathbf{n}_1, \tag{49}$$

$$\mathbf{x}_4^* = (\alpha + \gamma)\mathbf{n}_1, \tag{50}$$

The parameter γ controls the amplitude of the oscillators in the hidden attractor as well as the location of the two self-excited attractors, the parameter b controls the frequency in all the attractors, and a controls the time spent by a trajectory in each atom.

Assumption 1. *The parameters α, γ fulfill the expression $\frac{\gamma}{\alpha} \geq 10$. Since γ modifies the separation between attractors, it must be greater than α.*

Note that if $\alpha \neq 0$ and $\gamma = 0$ then the system has only two equilibria $\mathbf{x}_1^* = \mathbf{x}_3^*$ and $\mathbf{x}_2^* = \mathbf{x}_4^*$. And if $\gamma \neq 0$, then the system has four different equilibria, $\mathbf{x}_1^* \neq \mathbf{x}_2^* \neq \mathbf{x}_3^* \neq \mathbf{x}_4^*$. These equilibria can be separated by the γ parameter and are located around the points $-\gamma\mathbf{n}_1$ and $\gamma\mathbf{n}_1$. Two double-scroll self-excited attractors are generated around equilibria $\mathbf{x}_1^*$ and $\mathbf{x}_2^*$, and the other around equilibria $\mathbf{x}_3^*$ and $\mathbf{x}_4^*$. In [35] is presented a study of basins of attraction of a dynamical system that generates two double-scroll self-excited attractors and by separating its equilibria by pairs, it is possible to get two convex basins of attraction. In our study, we obtain two convex attracting basins when $\frac{\gamma}{\alpha} \geq 10$ and the space between these two attracting basins allows for a hidden attractor to emerge. On the other hand, when this ratio decreases, the two attracting basins are non-convex and entangled among them. For the appropriate selection of parameters a, b, c, α, and γ, the system exhibits three chaotic attractors, with two of them being self-excited and one hidden. Moreover, the self-excited attractors present Shilnikov chaos, which can be analytically proven.

Proposition 2. *Given a system of the form* (1), (2), (3), *and* (37), *there exist two heteroclinic cycles whose intersection points with the switching surfaces are given by*

$$\mathbf{x}_{in_1} = -\alpha\begin{bmatrix}1 & \frac{2c+a}{3} & \frac{2c^2-b^2+a^2}{3}\end{bmatrix}^T - \gamma\mathbf{n}_1, \tag{51}$$

$$\mathbf{x}_{in_2} = \alpha\begin{bmatrix}1 & \frac{2c+a}{3} & \frac{2c^2-b^2+a^2}{3}\end{bmatrix}^T - \gamma\mathbf{n}_1, \tag{52}$$

$$\mathbf{x}_{in_3} = -\alpha\begin{bmatrix}1 & \frac{2c+a}{3} & \frac{2c^2-b^2+a^2}{3}\end{bmatrix}^T + \gamma\mathbf{n}_1, \tag{53}$$

$$\mathbf{x}_{in_4} = \alpha\begin{bmatrix}1 & \frac{2c+a}{3} & \frac{2c^2-b^2+a^2}{3}\end{bmatrix}^T + \gamma\mathbf{n}_1, \tag{54}$$

Proof. The equilibria $\mathbf{x}_1^*$ and $\mathbf{x}_2^*$ are symmetric with respect to $-\gamma\mathbf{n}_1$ and $\mathbf{x}_3^*$ and $\mathbf{x}_4^*$ are symmetric with respect to $\gamma\mathbf{n}_1$; therefore, the proof for the heteroclinic cycle from $\mathbf{x}_1^*$ to $\mathbf{x}_2^*$ can be performed as the previous proof using the transformation

$$\mathbf{z}^{(\mathbf{i})} = Q^{-1}(\mathbf{x} - \mathbf{x}_i^*) \text{ for } i \in \{1,2,3,4\}, \tag{55}$$

and using SW_1 from (41). By symmetry, the heteroclinic cycle between $\mathbf{x}_3^*$ and $\mathbf{x}_4^*$ is also demonstrated by replacing SW_1 by SW_3. □

To illustrate a heteroclinic cycle, let us choose $a = 0.2$, $b = 5$, $c = -3$, $\gamma = 10$, and $\alpha = 1$.

In Figure 3, both heteroclinic cycles are shown. In Figure 4, the self-excited attractors are shown, with green for the initial condition $\mathbf{x}(0) = -\gamma\mathbf{n}_1$ and red for the initial condition $\mathbf{x}(0) = \gamma\mathbf{n}_1$. Figure 4 also shows the hidden attractor for the initial condition at the origin around the two self-excited attractors. Figure 5 shows a slice of the basin of attractions in the plane $\{\mathbf{x} \in \mathbb{R}^3 \mid 75.73x_1 + 0.33x_2 - 1.66x_3 = 0\}$.

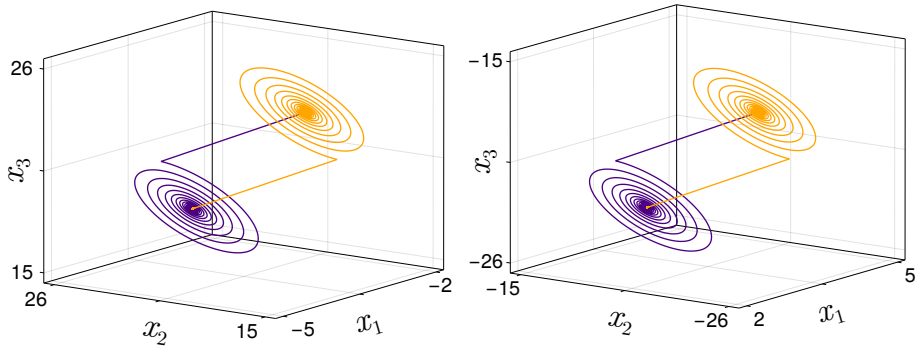

(**a**) (**b**)

Figure 3. Heteroclinic cycles of the system given by (1), (2), (3), (37), and (38) for the parameters $a = 0.2$, $b = 5$, $c = -3$, $\gamma = 10$, and $\alpha = 1$ located around (**a**) $\mathbf{x}(0) = -\gamma \mathbf{n}_1$ and (**b**) $\mathbf{x}(0) = \gamma \mathbf{n}_1$.

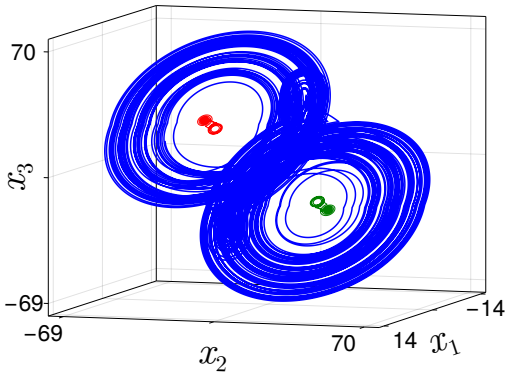

Figure 4. In blue is the hidden attractor and in red and green are the self-excited attractors of the system given by (1), (3), (2), (37), and (38) with $a = 0.2$, $b = 5$, $c = -3$, $\gamma = 10$, and $\alpha = 1$.

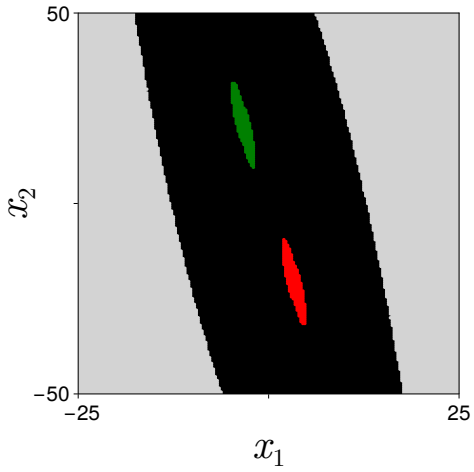

Figure 5. Slice of the computed basin of attraction in the plane $\{\mathbf{x} \in \mathbb{R}^3 \mid 75.73x_1 + 0.33x_2 - 1.66x_3 = 0\}$ of the system given by (1), (3), (2), (37), and (38) with $a = 0.2$, $b = 5$, $c = -3$, $\gamma = 10$, and $\alpha = 1$. In black is the basin of attraction of the hidden attractor. In red and green are the basins of attraction of the self-excited attractors.

4. 1D Grid Scroll Attractors

Now in order to generalize the approach for multistable systems with 1D hidden grid scroll attractors, let $X \subset \mathbb{R}^3$ and $P = \{P_1, \ldots, P_\eta\}$ $(\eta > 1)$ with $X = \bigcup_{1 \leq i \leq \eta} P_i$ and

$P_i \cap P_j = \emptyset$ for $i \neq j$ be a partition. Let us also consider that there exists a saddle equilibrium point in each atom P_i. Let us also redefine the function f_1 as follows:

$$f1 = \sum_{j=1}^{j=N_1} \gamma u((\mathbf{x} + (-2\gamma(j-1) + \gamma(N_1 - 1))\mathbf{n}_1)^T \mathbf{n}_\gamma), \tag{56}$$

where $N_1 + 1$ determines the number of scrolls in the hidden attractor.

Thus, the equilibria are located at

$$\mathbf{x}_i^* = (\gamma(-N_1 + 2\lfloor \frac{i}{2} \rfloor) + \alpha(-1)^i)\mathbf{n}_1, \tag{57}$$

for $i = \{0, \ldots, 2N_1 + 1\}$.

To illustrate this, we consider the same set of parameters with $N_1 = 3$, the hidden attractor (in blue) along with the four self-excited attractors (in different colors), as shown in Figure 6. Figure 7 shows a slice of the basin of attractions in the plane $\{\mathbf{x} \in \mathbb{R}^3 \mid 75.73x_1 + 0.33x_2 - 1.66x_3 = 0\}$. This surface was selected because it includes the line that passes through the central part of the self-excited attractors.

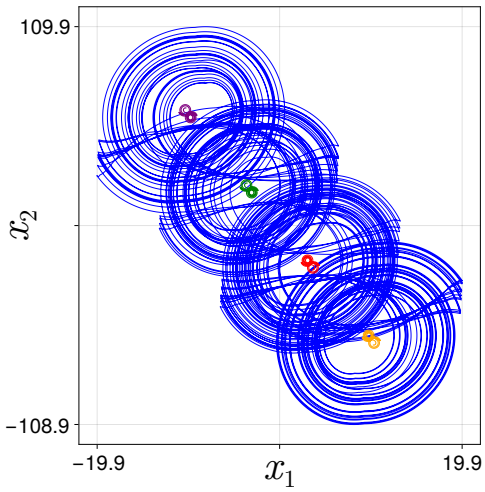

Figure 6. System given by (1), (3), (2), (37), and (56) with $a = 0.2$, $b = 5$, $c = -3$, $\gamma = 10$, and $\alpha = 1$.

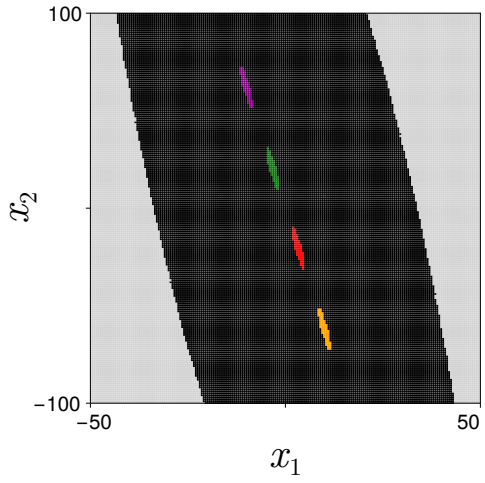

Figure 7. Slice of the computed basin of attraction in the plane $\{\mathbf{x} \in \mathbb{R}^3 \mid 75.73x_1 + 0.33x_2 - 1.66x_3 = 0\}$ of the system given by (1), (3), (2), (37), and (56) with $a = 0.2$, $b = 5$, $c = -3$, $\gamma = 10$, and $\alpha = 1$. In black is the basin of attraction of the hidden attractor. In red, green, orange, and purple are the basins of attraction of the self-excited attractors.

5. 2D and 3D Grid Scroll Attractors

For the generalization of 2D and 3D grids, let us redefine the system as

$$\dot{\mathbf{x}} = A\mathbf{x} + B(\mathbf{x}), \tag{58}$$

and consider the following vectors:

$$\begin{aligned} B_1 &= -\tfrac{1}{3}\begin{bmatrix} 2c-a \\ 2c^2+b^2-a^2 \\ 2c^3+3ab^2-a^3 \end{bmatrix}, \\ B_2 &= \begin{bmatrix} b \\ 2ab \\ 3a^2b-b^3 \end{bmatrix}, \\ B_3 &= -\tfrac{1}{3}\begin{bmatrix} 2c+2a \\ 2c^2-2b^2+2a^2 \\ 2c^3-6ab^2+2a^3 \end{bmatrix}, \end{aligned} \tag{59}$$

$$\mathbf{n}_{sw_2} = -\frac{1}{3}\begin{bmatrix} -(2ac^2+(2b^2-2a^2)c) \\ 2c^2+2b^2-2a^2 \\ 2c-2a \end{bmatrix} \tag{60}$$

$$\mathbf{n}_{sw_3} = \frac{1}{3}\begin{bmatrix} 2bc^2-4abc+b^3+a^2b \\ 2ab \\ -b \end{bmatrix}, \tag{61}$$

$$\mathbf{n}_2 = \frac{1}{3}\begin{bmatrix} 0 \\ -b \\ -2ab \end{bmatrix}. \tag{62}$$

The affine part of the system is given by

$$B(\mathbf{x}) = \left(f_4 + f_1 + \frac{wf_2}{\gamma}\right)B_1 + f_2B_2 + \left(f_3 - \frac{wf_2}{\gamma}\right)B_3, \tag{63}$$

with

$$f_2 = E_2\left(\sum_{k=1}^{N_2} \gamma u\left(\mathbf{n}_{sw_2}^T(\mathbf{x} - \mathbf{n}_2(2\gamma(k-1) - \gamma(N_2-1)))\right)\right), \tag{64}$$

$$f_3 = E_3\left(\sum_{l=1}^{N_3} \gamma u\left(\mathbf{n}_{sw_3}^T\left(\mathbf{x} - \mathbf{n}_3\left(-\frac{wf_2}{\gamma} + 2\gamma(l-1) - \gamma(N_3-1)\right)\right)\right)\right), \tag{65}$$

$$f_1 = \sum_{j=1}^{N_1} \gamma u\left(\mathbf{n}_\gamma^T\left(\mathbf{x} - \mathbf{n}_1\left(\frac{wf_2}{\gamma} + 2\gamma(j-1) - \gamma(N_1-1)\right)\right)\right), \tag{66}$$

$$f_4 = \alpha g\left(\mathbf{n}_\alpha^T\left(\mathbf{x} - \mathbf{n}_1\left(\frac{wf_2}{\gamma} + f_1\right) - \mathbf{n}_2f_2 - \mathbf{n}_3\left(-\frac{wf_2}{\gamma} + f_3\right)\right), \mathbf{n}_{sw_3}^T\left(\mathbf{x} - \mathbf{n}_3\left(-\frac{wf_2}{\gamma} + f_3\right)\right)\right), \tag{67}$$

where $\alpha, \gamma > 0$ and $\gamma/\alpha \geq 10$, $w \leq 0$ and $E_2, E_3 \in \{0, 1\}$.

With this modification of the approach, 1D, 2D, and 3D hidden scroll attractors can be obtained. It is possible to select which type of grid is desired, as shown in Table 1.

Table 1. Behavior of system (59) depending on the value of E2 and E3.

E2	*E3*	**Type of Hidden Grid Attractor.**
0	0	Scrolls along $\mathbf{n}_1$ direction (1D)
1	0	Scrolls along $\mathbf{n}_1$ and $\mathbf{n}_2$ directions (2D)
1	1	Scrolls along $\mathbf{n}_1$, $\mathbf{n}_2$, and $\mathbf{n}_3$ directions (3D)

Thus, the number of self-excited attractors as well as the scrolls in the hidden attractor is given by $(N_1+1)\times(E_2N_2+1)\times(E_3N_3+1)$.

Let us denote the equilibria along the x_1 axis as

$$\mathbf{x}^{*1D}_{eq_j} = (x^{*1D}_{1eq_j}, x^{*1D}_{2eq_j}, x^{*1D}_{3eq_j})^T,\ j = 1\ldots, 2N_1+2, \tag{68}$$

then the equilibria is given by

$$\mathbf{x}^{*3D}_{jkl} = \mathbf{x}^{*1D}_{eq_j} + \frac{wf_2}{\gamma}\mathbf{n}_1 + ((2kE_2 - N_2)\gamma + \frac{wf_2}{\gamma})\mathbf{n}_2 + (2lE_3 - N_3)\gamma\mathbf{n}_3, \tag{69}$$

with $k = 1,\ldots,2N_2+2$ y $l = 1,\ldots,2N_3+2$.

As an example of a 2D grid hidden attractor with scrolls along with the x_1 and x_2 directions, let us consider $a = 0.2$, $b = 5$, $c = -3$, and $w = -0.25$ with $E_2 = 1$, $E_3 = 0$, $N_{x_1} = 3$, and $N_3 = 3$. The hidden attractor is shown in Figure 8a. For a 3D grid case, consider the parameters $a = 0.2$, $b = 5$, $c = -7$, and $w = -1$ with $E_2 = 1$, $E_3 = 1$, $N_1 = 3$, and $N_3 = 3$, where the scrolls extend along three directions as shown in the Figure 8b. The resulting matrix A for this set of parameters is

$$A = \begin{bmatrix} 0 & 1 & 0 \\ 0 & 0 & 1 \\ -175.28 & -22.24 & -6.6 \end{bmatrix}. \tag{70}$$

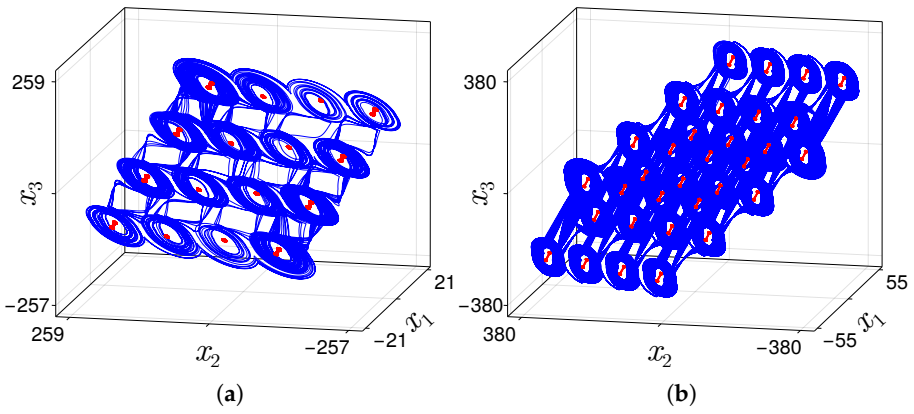

Figure 8. 2D grid hidden attractor of the system given by (58) and (2) with $a = 0.2$, $b = 5$, $c = -7$, $w = -0.5$, $N_1 = 3$, and $N_2 = 3$ with (**a**) $E_2 = 1$ and $E_3 = 0$ and (**b**) 3D grid hidden attractor of the system given by (58) and (2) with $a = 0.2$, $b = 5$, $c = -7$, $w = -0.5$, $N_1 = 3$, $N_2 = 3$, and $N_3 = 3$ with (**a**) $E_2 = 1$ and $E_3 = 1$

6. Generation of Pseudorandom Numbers Based on Hidden Attractors

The previous system with a 3D grid hidden attractor is used to generate binary sequences with the approach proposed in [31]. The algorithm has been chosen for its simplicity; however, more recent algorithms may produce better results. Two datasets were generated, one with the 3D grid hidden attractor and another with one of the self-excited double-scroll attractors. The algorithm requires a system trajectory obtained using

a numerical method with n points of the form $\mathbf{x_i} = [x_{1i}, x_{2i}, x_{3i}]^T$. Each point generates a byte as follows:

$$k_i = \left\lfloor \sum_{i=1}^{3} x_{1i} \cdot 10^{14} \right\rfloor \text{mod} 256, \tag{71}$$

such that $k_i \in [0, 255]$ for $i = 1, \ldots n$. The generated datasets were tested in the test suite provided by the National Institute of Standards and Technology (NIST).

The test suite includes fifteen statistical tests, and some of them are further decomposed into a variety of sub-tests. The NIST software (Statistical Test Suite sts-2.1.2) returns the called p-value and proportion, as well as an acceptable interval for these values; if the values of all tests are in the acceptance interval, the sequence is considered to be a pseudorandom number sequence. Both datasets fulfill all tests as shown in Table 2. Equation (71) is a simple way to generate pseudorandom numbers using bytes. It is worth noting that stream ciphers are based on pseudorandom numbers such as Salsa20 [36] and ChaCha [37].

Table 2. NIST test suite results.

		Self-Excited Attractor			Hidden Attractor		
Test No.	**Test Short Name**	***p*-Value**	**Proportion**	**Result**	***p*-Value**	**Proportion**	**Result**
1	Frequency	0.214	0.988	Pass	0.273	0.987	Pass
2	BlockFrequency	0.748	0.989	Pass	0.339	0.988	Pass
3	CumulativeSums *	0.154	0.985	Pass	0.167	0.984	Pass
4	Runs	0.237	0.998	Pass	0.256	0.989	Pass
5	LongestRun	0.512	0.986	Pass	0.130	0.990	Pass
6	Rank	0.668	0.995	Pass	0.838	0.989	Pass
7	FFT	0.504	0.981	Pass	0.035	0.986	Pass
8	NonOverlappingTemplate *	0.992	0.983	Pass	0.677	0.985	Pass
9	OverlappingTemplate	0.532	0.994	Pass	0.237	0.994	Pass
10	Universal	0.450	0.985	Pass	0.053	0.988	Pass
11	ApproximateEntropy	0.672	0.988	Pass	0.405	0.991	Pass
12	RandomExcursions *	0.448	0.989	Pass	0.681	0.986	Pass
13	RandomExcursionsVariant *	0.329	0.986	Pass	0.993	0.981	Pass
14	Serial *	0.283	0.990	Pass	0.0.643	0.987	Pass
15	LinearComplexity	0.973	0.991	Pass	0.885	0.992	Pass

* Worst proportion case from all sub-tests.

7. Conclusions

This study addresses a new approach for the design of multistable systems with multiple self-excited attractors and a hidden scroll attractor which can exhibit a 1D, 2D, or 3D grid shape. Several known system constructions for multiscroll attractors present a limitation, which is the set of eigenvalues of the main matrix that can produce a scroll attractor. This drawback is imposed by the shape of the main matrix of the vector field along with the static commutation planes, which reduces the flexibility of design. This approach presented in this study eliminates this limitation and guarantees the existence of chaos in the Shilnikov sense in all self-excited attractors, maintaining the same matrix shape. Although a particular case constructed with this approach was used to generate binary sequences that fulfill the NIST tests, further studies are required to ensure proper use in an encryption application. Future work could address the design of a sequence generator specifically designed for these types of systems.

Author Contributions: Conceptualization, R.d.J.E.-G., H.E.G.-V., and E.C.; methodology, R.d.J.E.-G., H.E.G.-V., and E.C.; formal analysis, R.d.J.E.-G., H.E.G.-V., and E.C.; writing—review and editing, R.d.J.E.-G., H.E.G.-V., and E.C.; supervision, E.C. All authors have read and agreed to the published version of the manuscript.

Funding: This research received no external funding.

Data Availability Statement: Data is contained within the article.

Acknowledgments: R. J. Escalante-González thanks SECIHTI for the financial support of the SNII.

Conflicts of Interest: The authors declare no conflicts of interest.

References

1. Ghys, É. The Lorenz attractor, a paradigm for chaos. In *Chaos: Poincaré Seminar 2010*; Springer: Basel, Switzerland, 2013; pp. 1–54.
2. Chowdhury, S.N.; Anwar, M.S.; Ghosh, D. Cluster formation due to repulsive spanning trees in attractively coupled networks. *Phys. Rev. E* **2024**, *109*, 044314. [CrossRef]
3. Chowdhury, S.N.; Meyer-Ortmanns, H. Topologically protected edge oscillations in nonlinear dynamical units. *Phys. Rev. E* **2025**, *112*, 044204. [CrossRef]
4. Chowdhury, S.N.; Kundu, S.; Banerjee, J.; Perc, M.; Ghosh, D. Eco-evolutionary dynamics of cooperation in the presence of policing. *J. Theor. Biol.* **2021**, *518*, 110606. [CrossRef] [PubMed]
5. Cantón, E.C.; González, R.d.J.E.; Velázquez, H.E.G. *Generation of Self-Excited, Hidden and Non-Self-Excited Attractors in Piecewise Linear Systems: Some Recent Approaches*; World Scientific: Singapore, 2023.
6. Piórek, M. *Analysis of Chaotic Behavior in Non-Linear Dynamical Systems*; Springer International Publisher: Berlin/Heidelberg, Germany, 2019.
7. Guan, X.; Xie, Y. A review on methods for localization of hidden attractors: X. Guan, Y. Xie. *Nonlinear Dyn.* **2025**, *113*, 22223–22255. [CrossRef]
8. Chowdhury, S.N.; Ghosh, D. Hidden attractors: A new chaotic system without equilibria. *Eur. Phys. J. Spec. Top.* **2020**, *229*, 1299–1308. [CrossRef]
9. Leonov, G.; Kuznetsov, N.; Vagaitsev, V. Localization of hidden Chua's attractors. *Phys. Lett. A* **2011**, *375*, 2230–2233. [CrossRef]
10. Dudkowski, D.; Jafari, S.; Kapitaniak, T.; Kuznetsov, N.V.; Leonov, G.A.; Prasad, A. Hidden attractors in dynamical systems. *Phys. Rep.* **2016**, *637*, 1–50. [CrossRef]
11. Gao, F.; Yu, X.; Deng, Y.; Yuan, F.; Wang, G.; Lei, T. Memristive Effect on a Hindmarsh-Rose Neuron. *Chin. Phys. B* **2025**, *34*, 120504. [CrossRef]
12. Luo, M.; Wang, P.; Qiu, D.; Zhang, B.; Liu, S. Analysis and application of conditionally symmetric memristive chaotic systems with attractor growth phenomena. *Chaos Solitons Fractals* **2025**, *200*, 117027. [CrossRef]
13. Pan, J.; Wang, H.; Hu, F. Creation of hidden *n*-scroll Lorenz-like attractors. *Electron. Res. Arch.* **2025**, *33*, 4167–4183. [CrossRef]
14. Kuznetsov, N.; Leonov, G. Numerical Visualization of attractors: Self-exciting and hidden attractors. In *Handbook of Applications of Chaos Theory*; CRC: Boca Raton, FL, USA, 2016; pp. 135–143.
15. Suykens, J.A.; Huang, A.; Chua, L.O. A family of n-Scroll attractors from a generalized Chua's Circuit. *Arch. Elektron. Ubertragung-stechnik* **1997**, *51*, 131–138.
16. Tang, K.S.W.; Chen, G.; Zhong, G.Q.; Man., K.F. Generation of N-Scroll attractors via sine function. *IEEE Trans. Circuits Syst. Fundam. Theory Appl.* **2001**, *48*, 1369–1372. [CrossRef]
17. Yalçin, M.E.; Suykens, J.A.K.; Vandewalle, J. Families of scroll grid attractors. *Int. J. Bifurc. Chaos* **2002**, *12*, 23–41. [CrossRef]
18. Gilardi-Velázquez, H.E.; Ontañón-García, L.; Hurtado-Rodriguez, D.G.; Campos-Cantón, E. Multistability in piecewise linear systems versus eigenspectra variation and round function. *Int. J. Bifurc. Chaos* **2017**, *27*, 1730031. [CrossRef]
19. Anzo-Hernández, A.; Gilardi-Velázquez, H.E.; Campos-Cantón, E. On multistability behavior of unstable dissipative systems. *Chaos Interdiscip. J. Nonlinear Sci.* **2018**, *28*, 033613. [CrossRef]
20. Pham, V.T.; Vaidyanathan, S.; Volos, C.; Jafari, S.; Kingni, S.T. A no-equilibrium hyperchaotic system with a cubic nonlinear termViet. *Optik* **2016**, *127*, 3259–3265. [CrossRef]
21. Gilardi-Velázquez, H.E.; Escalante-González, R.d.J.; Campos-Cantón, E. Bistable behavior via switching dissipative systems with unstable dynamics and its electronic design. *IFAC-PapersOnLine* **2018**, *51*, 502–507. [CrossRef]
22. Gilardi-Velázquez, H.E.; Escalante-González, R.J.; Campos, E. Emergence of a square chaotic attractor through the collision of heteroclinic orbits. *Eur. Phys. J. Spec. Top.* **2020**, *229*, 1351–1360. [CrossRef]
23. Echenausía-Monroy, J.L.; Huerta-Cuellar, G.; Jaimes-Reátegui, R.; García-López, J.H.; Aboites, V.; Cassal-Quiroga, B.B.; Gilardi-Velázquez, H.E. Multistability emergence through fractional-order-derivatives in a PWL multi-scroll system. *Electronics* **2020**, *9*, 880. [CrossRef]
24. Echenausía-Monroy, J.; Gilardi-Velázquez, H.E.; Wang, N.; Jaimes-Reátegui, R.; García-López, J.; Huerta-Cuellar, G. Multistability route in a PWL multi-scroll system through fractional-order derivatives. *Chaos Solitons Fractals* **2022**, *161*, 112355. [CrossRef]
25. Munoz-Pacheco, J.M.; Zambrano-Serrano, E.; Volos, C.; Jafari, S.; Kengne, J.; Rajagopal, K. A New Fractional-Order Chaotic System with Different Families of Hidden and Self-Excited Attractors. *Entropy* **2018**, *20*, 564. [CrossRef] [PubMed]

26. Yu, F.; Kong, X.; Yao, W.; Zhang, J.; Cai, S.; Lin, H.; Jin, J. Dynamics analysis, synchronization and FPGA implementation of multiscroll Hopfield neural networks with non-polynomial memristor. *Chaos Solitons Fractals* **2024**, *179*, 114440. [CrossRef]
27. He, T.; Yu, F.; Lin, Y.; He, S.; Yao, W.; Cai, S.; Jin, J. Multi-scroll Hopfield neural network excited by memristive self-synapses and its application in image encryption. *Chin. Phys. B* **2025**, *34*, 120506. [CrossRef]
28. Feng, W.; Tang, Z.; Zhao, X.; Qin, Z.; Chen, Y.; Cai, B.; Zhu, Z.; Qian, K.; Wen, H. Two-Dimensional Coupling-Enhanced Cubic Hyperchaotic Map with Exponential Parameters: Construction, Analysis, and Application in Hierarchical Significance-Aware Multi-Image Encryption. *Axioms* **2025**, *14*, 901. [CrossRef]
29. Feng, W.; Tang, Z.; Zhao, X.; Qin, Z.; Chen, Y.C.B.; Zhu, Z.; Wen, H.; Ye, C. State-Dependent Variable Fractional-Order Hyperchaotic Dynamics in a Coupled Quadratic Map: A Novel System for High-Performance Image Protection. *Fractal Fract.* **2025**, *9*, 792. [CrossRef]
30. Li, H.; Yu, S.; Feng, W.; Chen, Y.; Zhang, J.; Qin, Z.; Zhu, Z.; Wozniak, M. Exploiting Dynamic Vector-Level Operations and a 2D-Enhanced Logistic Modular Map for Efficient Chaotic Image Encryption. *Entropy* **2023**, *25*, 1147. [CrossRef] [PubMed]
31. García-Martínez, M.; Ontañón-García, L.; Campos-Cantón, E.; Čelikovský, S. Hyperchaotic encryption based on multi-scroll piecewise linear systems. *Appl. Math. Comput.* **2015**, *270*, 413–424. [CrossRef]
32. Gilardi-Velázquez, H.E.; Echenausia-Monroy, J.; Escalante-González, R.; Campos, E. Codification of Images Based on Deterministic Brownian Motion. In *Chaotic Modeling and Simulation International Conference*; Springer: Cham, Switzerland, 2023; pp. 143–156.
33. Jin, X.; Duan, X.; Jin, H.; Ma, Y. A Novel Hybrid Secure Image Encryption Based on the Shuffle Algorithm and the Hidden Attractor Chaos System. *Entropy* **2020**, *22*, 640. [CrossRef]
34. Stitt, M. Designing with op amps: Single-formula technique keeps it simple. *EDN* **1998**, *43*, 135–137.
35. Ontañón-García, L.; Campos-Cantón, E. Widening of the basins of attraction of a multistable switching dynamical system with the location of symmetric equilibria. *Nonlinear Anal. Hybrid Syst.* **2017**, *26*, 38–47. [CrossRef]
36. Bernstein, D.J. *Salsa20 Design*; Technical Report 2005/025, eSTREAM, ECRYPT Stream Cipher Project. 2005. Available online: https://www.google.com/url?sa=t&source=web&rct=j&opi=89978449&url=https://cr.yp.to/snuffle/design.pdf&ved=2ahUKEwjCxtffk_SSAxUO4zQHHRXYCVMQFnoECCEQAQ&usg=AOvVaw1Le-XlukKqZraSr7XjWAvm (accessed on 12 February 2026).
37. Bernstein, D.J. ChaCha, a variant of Salsa20. In Proceedings of the SASC 2008: The State of the Art of Stream Ciphers. ECRYPT, Lausanne, Switzerland, 13–14 February 2008. Available online: https://cr.yp.to/chacha/chacha-20080120.pdf (accessed on 12 February 2026).